

Simulation of air pollution propagation in a street canyon

R.B. Nuterman and A.V. Starchenko

Tomsk State University

Received January 24, 2005

The results of numerical simulation of pollutant transport over a surface with large-scale roughness are presented. The problem was solved with the use of the Reynolds-averaged Navier–Stokes equations with the Boussinesq closure. Turbulent parameters were determined on the basis of the modified k – ε -model of turbulence and the Launder–Spalding’s method of wall functions. The problem is solved numerically by the finite-volume method. The influence of urban vegetation on air pollution and the effect of traffic-induced turbulence on the pathways of air pollutants in a street canyon were investigated.

Introduction

Traffic is now one of the main sources of air pollution in cities.¹ Many components of vehicle emissions, for example, benzopyrene, are very harmful for the human health. Therefore, the determination of harmful substance concentrations in a city, study of causes, and prevention of conditions for the increased level of pollution of the surface air are urgent problems.

One of the methods of investigation of pollutant transport in the urban environment is the mathematical simulation based on the use of equations of fluid dynamics and turbulent diffusion. Thus, in Ref. 2, to determine the structure of a turbulent flow in an extended street canyon, the Reynolds equation and the k – ε -model of turbulence in the two-dimensional formulation were applied. It has been found numerically that the vortex motion is formed inside the street canyon, and the center of this motion shifts towards its windward side depending on the wind strength and canyon configuration. The results of experimental and theoretical investigation of the pollutant concentration distribution in the street canyon as a function of the wind direction were presented in Ref. 3. The analysis has revealed that the pollutant concentration on the leeward side of the street canyon is much higher than on the windward side.

A team of European scientists, working within the TRAPOS Projects, has now developed a series of models, such as CHENSI-1, CHENSI-2, MIMO, MISKAM, and TASCflow for calculation of spreading harmful pollutants emitted by traffic.⁴ The basic equations for these models are the nonstationary Reynolds equations for representation of the averaged turbulent motion. For closure of these equations, the k – ε or k – ω model of turbulence or some of its versions are used. The convection–diffusion equation serves a transport equation for description of pollutant dispersion. All the models (except for TASCflow) are

realized numerically on a staggered grid. In the CHENSI-1 model, differential equations are solved by the finite-difference method, while the method of finite volume is employed for this purpose in CHENSI-2, MIMO, and MISKAM. In the TASCflow model, the equations are solved by the method of finite elements. These models can be used to study the spread of pollutants both in an individual street canyon, and in blocks.

The aim of this work is to construct a mathematical model of the air turbulent motion and pollutant transport in an extended street canyon, as well as to study the influence of the configuration of urban elements and limited areas of vegetation on aerodynamics of the pollutant flow and the level of pollution in atmospheric air.

Formulation of the problem

A two-dimensional turbulent isothermal motion of air over some surface with elements of large-scale roughness is considered.

The roughness elements are rectangular obstacles, whose size is comparable with the size of the region under study. Two types of obstacles are considered: buildings impenetrable for airflows, and penetrable vegetation areas or individual trees. The motion has a stationary character.

The mathematical formulation of the problem includes the Reynolds-averaged Navier–Stokes equations, written with the use of the Boussinesq closure relations⁵

$$\frac{\partial U}{\partial x} + \frac{\partial V}{\partial y} = 0, \quad (1)$$

$$\begin{aligned} U \frac{\partial U}{\partial x} + V \frac{\partial U}{\partial y} = & -\frac{1}{\rho} \frac{\partial \tilde{P}}{\partial x} + 2 \frac{\partial}{\partial x} \left[(v + v_t) \frac{\partial U}{\partial x} \right] + \\ & + \frac{\partial}{\partial y} \left[(v + v_t) \frac{\partial U}{\partial y} \right] + \frac{\partial}{\partial y} \left[(v + v_t) \frac{\partial V}{\partial x} \right] - F_x, \quad (2) \end{aligned}$$

$$U \frac{\partial V}{\partial x} + V \frac{\partial U}{\partial y} = -\frac{1}{\rho} \frac{\partial \tilde{P}}{\partial y} + \frac{\partial}{\partial x} \left[(v + v_t) \frac{\partial V}{\partial x} \right] + 2 \frac{\partial}{\partial y} \left[(v + v_t) \frac{\partial V}{\partial y} \right] + \frac{\partial}{\partial x} \left[(v + v_t) \frac{\partial U}{\partial y} \right] - F_y. \quad (3)$$

Here U, V are wind velocity projections on the axes Ox and Oy ; ν is the kinematic viscosity of air; ν_t is the turbulent viscosity; $\tilde{P} = P + 2/3\rho k$, where P is pressure; k is the kinetic energy of turbulence; ρ is density; F_x, F_y are projections of resistance to the airflow in a vegetation area. The equations for F_x, F_y have the form

$$F_x = \eta C_f a U \sqrt{U^2 + V^2}, \quad F_y = \eta C_f a V \sqrt{U^2 + V^2},$$

where η is the fraction of the surface covered by trees; C_f is the coefficient of resistance; a is the density of trees in a forested areas (for example, for pine trees $\eta = 1, C_f = 0.2, a = 0.3125 \text{ m}^2/\text{m}^3$ (Ref. 6)).

The boundary conditions for the system of equations (1)–(3) are chosen as follows (Fig. 1):

– at the left boundary at $x = 0$:

$$U(0, y) = U_{300} \left(\frac{y - Ly_1}{300 - Ly_1} \right)^{0.3};$$

$$V(0, y) = 0;$$

– at the right boundary at $x = Lx$:

$$\frac{\partial U}{\partial x} = \frac{\partial V}{\partial x} = 0;$$

– at the lower boundary:

$$U = V = 0;$$

– at the upper boundary at $y = Ly$:

$$U = U_{300} \left(\frac{Ly - Ly_1}{300 - Ly_1} \right)^{0.3};$$

$$V = 0.$$

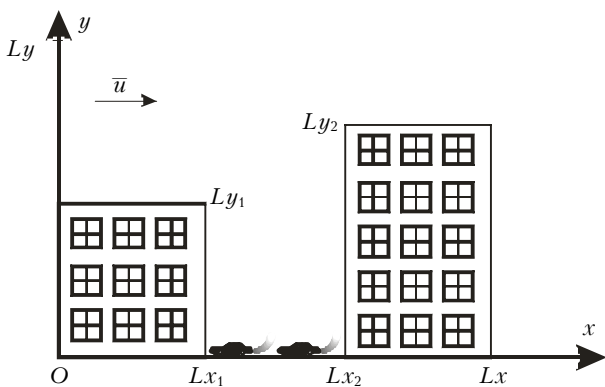


Fig. 1. Geometry of the region under study.

The concentration field of some gaseous inert pollutant is determined from solution of the transport equation, which has the form

$$\frac{\partial(UC)}{\partial x} + \frac{\partial(VC)}{\partial y} = \frac{\partial}{\partial x} \left[\left(\frac{\nu}{Sc} + \frac{\nu_t}{Sc_t} \right) \frac{\partial C}{\partial x} \right] + \frac{\partial}{\partial y} \left[\left(\frac{\nu}{Sc} + \frac{\nu_t}{Sc_t} \right) \frac{\partial C}{\partial y} \right] + I, \quad (4)$$

where C is the pollutant concentration; Sc is the Schmidt number; Sc_t is the turbulent Schmidt number; I is the source term, determining the intensity of pollutant inflow. In this work, the deposition of a gaseous pollutant emitted by traffic (for example, carbon monoxide) on streamline and penetrable obstacles is neglected, because the intensity of absorption of a gaseous pollutant in the street canyon with sparse plants is much lower than the rate of its emission by vehicles.¹ The differential equation (4) was integrated with the zero boundary condition for the pollutant concentration at the left boundary and simple gradient relations at other boundaries.

To determine the flow turbulent parameters, the $k-\varepsilon$ model of turbulence⁷ was used:

$$U \frac{\partial k}{\partial x} + V \frac{\partial k}{\partial y} = \frac{\partial}{\partial x} \left[\left(\nu + \frac{\nu_t}{\sigma_k} \right) \frac{\partial k}{\partial x} \right] + \frac{\partial}{\partial y} \left[\left(\nu + \frac{\nu_t}{\sigma_k} \right) \frac{\partial k}{\partial y} \right] + G - \varepsilon + F_k, \quad (5)$$

$$U \frac{\partial \varepsilon}{\partial x} + V \frac{\partial \varepsilon}{\partial y} = \frac{\partial}{\partial x} \left[\left(\nu + \frac{\nu_t}{\sigma_\varepsilon} \right) \frac{\partial \varepsilon}{\partial x} \right] + \frac{\partial}{\partial y} \left[\left(\nu + \frac{\nu_t}{\sigma_\varepsilon} \right) \frac{\partial \varepsilon}{\partial y} \right] + (c_1 G - c_2 \varepsilon) \frac{\varepsilon}{k} + F_\varepsilon; \quad (6)$$

$$\nu_t = c_\mu \frac{k^2}{\varepsilon}, \quad (7)$$

where ε is the energy of dissipation of the turbulence k ; the generation of the turbulence energy is described as

$$G = \nu_t \left[2 \left(\frac{\partial U}{\partial x} \right)^2 + 2 \left(\frac{\partial V}{\partial y} \right)^2 + \left(\frac{\partial U}{\partial y} + \frac{\partial V}{\partial x} \right)^2 \right];$$

and the constants are: $c_1 = 1.44, c_2 = 1.92, \sigma_k = 1.0, \sigma_\varepsilon = 1.3$. In Eqs. (5) and (6), F_k, F_ε are additional source terms, modeling the influence of plants on turbulence, which have the form:

$$F_k = UF_x + VF_y, \quad F_\varepsilon = \frac{\varepsilon}{k} C_{pe1} (UF_x + VF_y),$$

where $C_{pe1} = 2.0$ [Ref. 6]. Moving vehicles are not only sources of pollutant emissions into the

atmosphere, but also generators of the so-called mechanical turbulence, caused by the air disturbance as a result of motion of a finite-length objects having a significant resistance. In this work, this factor is taken into account (as in Ref. 8) by adding the corresponding terms into the k - ε model of turbulence. The results of calculations have shown that the addition of the mechanical turbulence to the model leads to increase of the role of the turbulent diffusion in the pollutant spreading under urban conditions due to the increased level of turbulence. To take into account the generation of the kinetic energy of turbulence due to the traffic, the right-hand side of Eq. (5) is complemented with the term $C_{\text{car}}V_{\text{car}}^2Q_{\text{car}}$, while Eq. (6) is complemented with the term responsible for the dissipation of the mechanical energy of turbulence, which has the form $C_{\text{car}}V_{\text{car}}^2Q_{\text{car}}(\varepsilon/k)$, where $C_{\text{car}} = 0.0015$ is the empirical coefficient; V_{car} is the vehicle speed; Q_{car} is the number of vehicles per second [Ref. 8].

In this paper, we consider two versions of the closure relation (7). In the first case, the coefficient c_μ is equal to 0.09, as in the original k - ε model.⁷ In the second case, the influence of the curvature of flow lines on the turbulent stress tangents and on the degree of anisotropy of normal stresses is taken into account⁹:

$$c_\mu = \frac{0.09}{\left[1 + 0.285 \frac{k^2}{\varepsilon^2} \frac{\partial U_s}{\partial n} U_{ss} \Omega\right]}, \quad (8)$$

where

$$\frac{\partial U_s}{\partial n} = U_{ss}\Omega + \Omega_1 \sin(2\theta) + (\Omega_2 + \Omega_3)\cos(2\theta).$$

In this case,

$$\begin{aligned} \Omega &= (\Omega_1 UV + \Omega_2 U^2 - \Omega_3 V^2) / U_{ss}^3, \\ \Omega_1 &= \frac{\partial V}{\partial y} - \frac{\partial U}{\partial x}, \quad \Omega_2 = \frac{\partial V}{\partial x}, \quad \Omega_3 = \frac{\partial U}{\partial y}; \\ \theta &= \arctan\left(\frac{U}{V}\right); \quad U_{ss} = \sqrt{U^2 + V^2}. \end{aligned}$$

The boundary conditions for Eqs. (5)–(7) have the form:

– at the left boundary at $x = 0$:

$$k = k_0(y), \quad \varepsilon = \varepsilon_0(y);$$

– at the right boundary at $x = Lx$:

$$\frac{\partial k}{\partial x} = \frac{\partial \varepsilon}{\partial x} = 0;$$

– at the upper boundary at $y = Ly$:

$$\frac{\partial k}{\partial y} = \frac{\partial \varepsilon}{\partial y} = 0.$$

To define the values of the turbulent parameters near surfaces of urban elements, the Launder–Spalding's method of wall functions⁷ is used. According to this method, the velocity component tangent to the surface near the surface can be represented as

$$U_\tau = \frac{\tau_w}{\rho c_\mu^{1/4} \kappa k^{1/2}} \ln \left[E c_\mu^{1/4} k^{1/2} n / \nu \right],$$

where $\kappa = 0.42$; $E = 9.0$; τ_w is the surface friction; n is the distance from the streamline surface. The kinetic energy of turbulence k near the surface (in a wall cell of the difference grid) is determined from Eq. (5) with the use of the following equations for the generation and dissipation of the turbulence energy:

$$G = \nu_t \frac{|\tau_w|}{\rho(\kappa n)^2}; \quad \varepsilon = \frac{\left[k c_\mu^{1/2} \right]^{3/2}}{\kappa n}.$$

Solution of the problem and calculated results

The problem is solved numerically on a uniform grid. The differential equations are discretized by the finite-volume method,¹⁰ and the convective terms of the transport equations are approximated with the use of the MLU scheme.¹¹ To calculate the integrals, piecewise-linear profiles, describing the function variation between nodes, are used.¹² This discretization yields the grid equations, which can be solved by the Buleev method of incomplete factorization.¹³ To match the pressure field to the velocity field, the Patankar–Spalding SIMPLE algorithm¹⁰ is used. To check the adequacy of the model and the method of solution, we have carried out a series of test calculations.

Test 1. Turbulent motion behind a ledge [Ref. 14]

The ledge height is $h = 0.076$ m, and the fluid velocity in the entrance cross section is 10 m/s. The flow pattern corresponds to the Reynolds number of 50 000. The calculations were carried out in a region with the dimensions of 2 m along the axis Ox and 0.4 m along the axis Oy on a 150×80 grid at $c_\mu = 0.09$ and with allowance for influence of the flow line curvature on the turbulent structure of the flow [c_μ is calculated by Eq. (8)]. Figures 2 and 3 show the vector field of the turbulent motion behind the ledge, the plot of variation of the pressure coefficient, the dimensionless velocity, and the kinetic energy of the turbulence downstream.

Calculations show that when using the standard k - ε model, the recirculating flow zone is smaller than it actually is. The modification of the turbulence model in order to take into account the influence of the flow line curvature on the turbulent structure allows more accurate calculation of the recirculating zone.

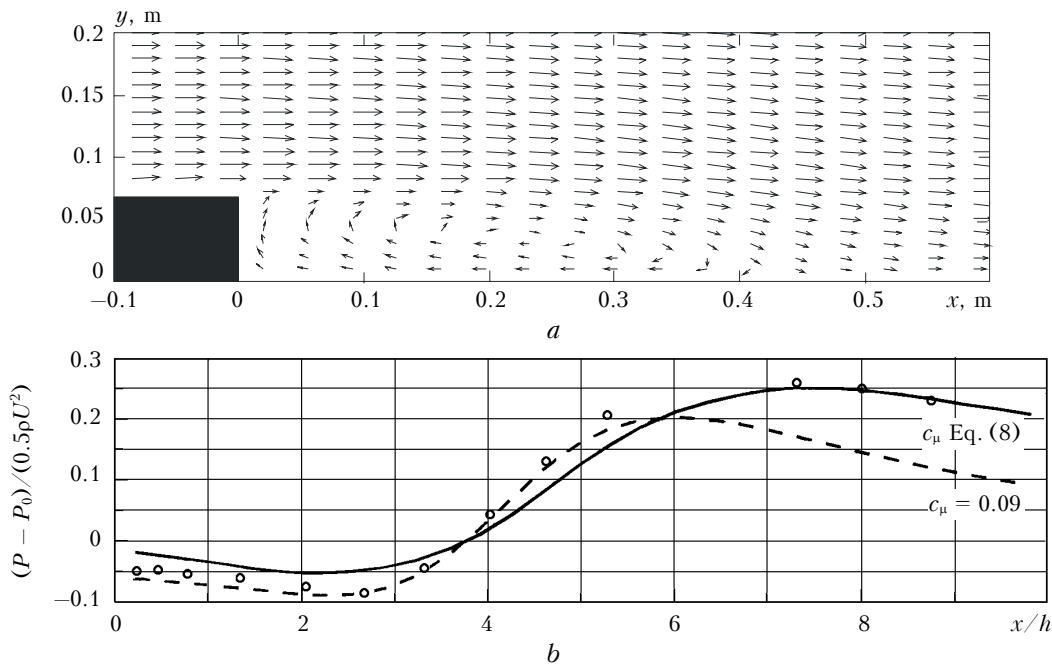


Fig. 2. Vector field of velocity in the case of flowing along a plate with a ledge (a); $Re = 50000$, $h = 0.076$ m (c_μ by Eq. (8)); distribution of the pressure coefficient behind a reward-facing ledge: experiment from Ref. 14 (o) (b).

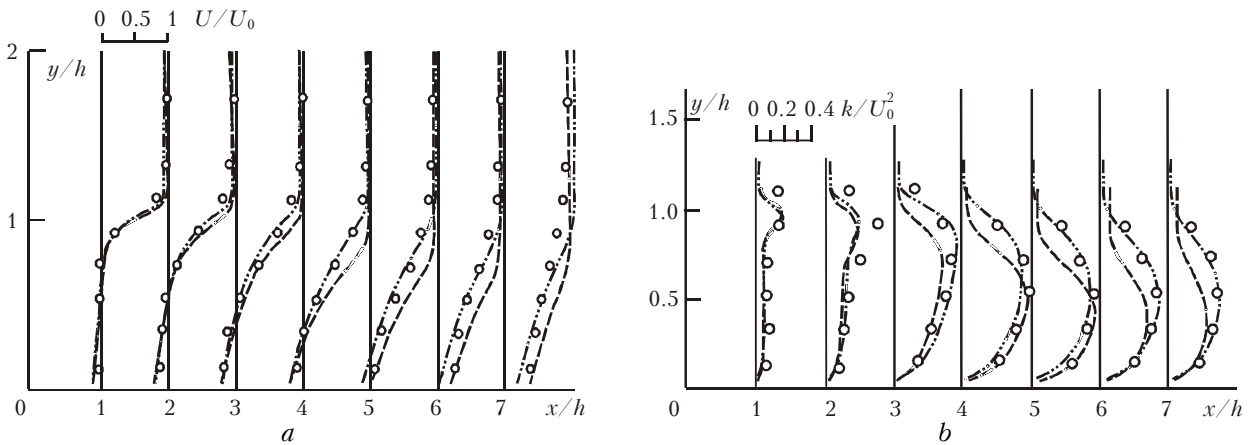


Fig. 3. Profiles of velocity and the kinetic energy of turbulence behind a ledge: $c_\mu = 0.09$ (---); c_μ is calculated by Eq. (8) (-.-.); experiment from Ref. 14 (o).

Test 2. Pollutant transport in a street canyon

The dimensionless concentration of a pollutant in the street canyon was calculated as a function of the wind direction, and the results obtained were compared with other similar model results and with experimental data from Ref. 4. The dimensionless concentration was determined as $c^* = C U_{H_{ref}} H / I$, where C_{left} is the concentration at the left wall of the canyon; $U_{H_{ref}}$ is the velocity at the height H_{ref} (for example, 100 m); H is the characteristic height (for example, mean height of buildings, equal to about 16 m), and I is the intensity of the source of pollution. The results were compared with those obtained by the following models: MISKAM 1.1 (two-dimensional Microscale Flow and Dispersion Model), MISKAM 3.51,

MISKAM 3.6 (three-dimensional Microscale Flow and Dispersion Models),¹⁵ and OSPM (Danish two-dimensional Operational Street Pollution Model).¹⁶ Figure 4 shows the results obtained for the canyon of an ideal shape with the width and height of 16 m and the length of 90 m. By the symmetry reasons, the results are shown only for directions from 90 to 270°; the direction of 180° corresponds to the flow parallel to the street.

The best agreement with the results in a wind tunnel⁴ was obtained for the MISKAM 1.1 model. The latest versions of this model predict both the overestimated concentrations in the windward side (90°, MISKAM. 3.51) and underestimated ones (in comparison with the experiment) on the leeward side (270°, MISKAM. 3.6). OSPM gives larger values, except for the direction of 270°, where the clearly

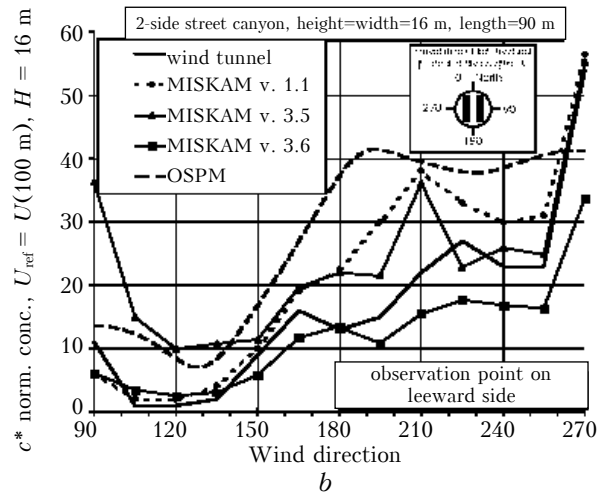
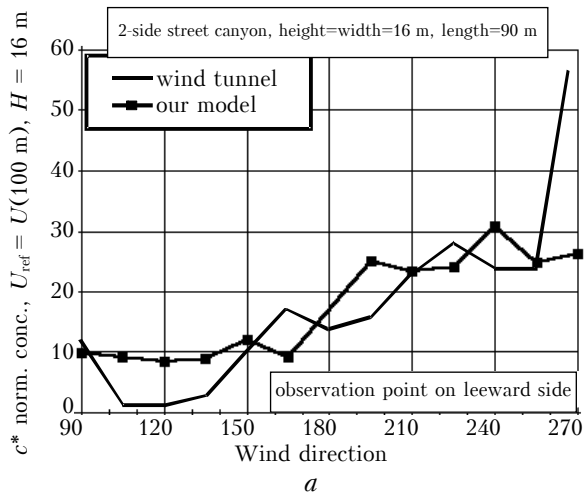


Fig. 4. Dimensionless concentration in a street canyon as a function of the wind direction: calculations by the Eqs. (1)–(8) (a); MISKAM, OSPM, and experiments in a wind tunnel¹⁶ (b).

pronounced maximum is not achieved. Analogous calculations by Eqs. (1)–(8) (the result is shown in Fig. 4a) clearly demonstrate that the concentration level is low on the windward side. It should be noted that, in general, the agreement with the experimental data from Ref. 4 is good.

Test 3. Air mass motion behind some isolated tree of height H

The region under study is shown in Fig. 5.

Figure 6 shows vertical profiles of the axial velocity and the kinetic energy of turbulence at different distances from some tree. The calculations show the processes of viscous dissipation to be prevailing in the vegetation area, therefore, the kinetic

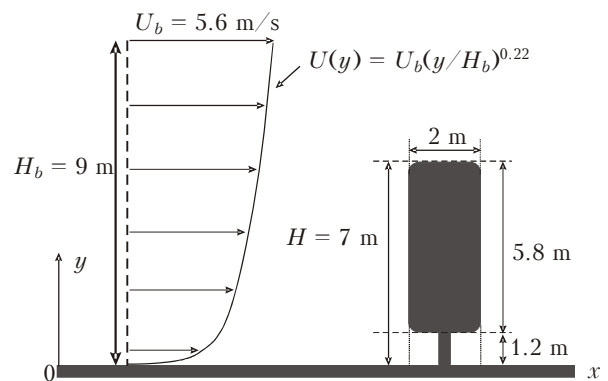


Fig. 5. Region of the study of air motion behind some isolated tree.

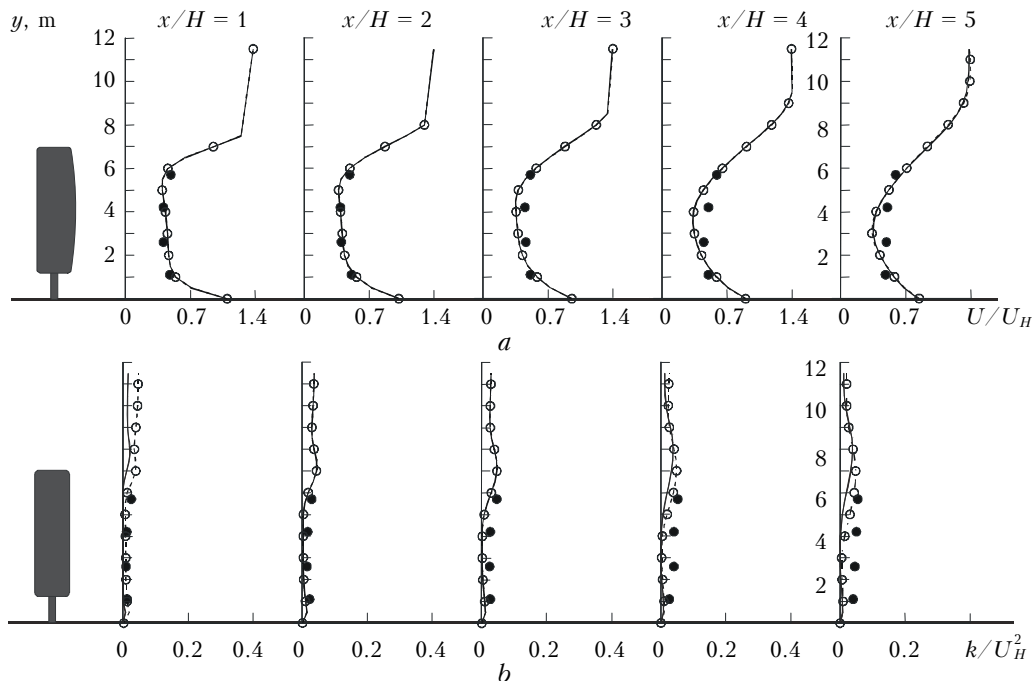


Fig. 6. Comparison of vertical profiles of velocity and kinetic energy behind a tree: experiment from Ref. 6 (●); $c_\mu = 0.09$ (—), c_μ calculated by Eq. (8) (○); U_H is the velocity at $y = H$.

energy of turbulence is minimal behind the tree. At the same time, because of significant velocity gradients in the upper part of the tree crown and above the tree, the turbulent transport intensity increases at this height. On the one hand, the resistance of the penetrable obstacle to the incoming flow leads to decrease of the velocity axial component behind the tree (Fig. 6). On the other hand, because the vegetation density is lower near the ground, the axial velocity here is higher (Fig. 6). In general, a good agreement with the measurements from Ref. 6 and with the physical pattern of the process described in Ref. 1 is observed. It should be also noted that, taking into account of the influence of the flow line curvature on the turbulent characteristics and the degree of anisotropy of normal stresses [Eq. (8)], it is possible to predict the kinetic energy distribution, which corresponds to the actual turbulent structure of the flow to the

higher extent than that obtained with the use of the standard $k-\epsilon$ model of turbulence.⁷

The proposed mathematical model was applied to the study of flow aerodynamics and the transport of a traffic pollutant in urban building elements. The calculations were carried out on a 161×121 grid. The pollution sources of constant intensity were located near the surface ($y = 0$) at a distance of 5 m from buildings (see Fig. 1). The velocity of the incoming flow was $U_{300} = 1$ m/s. In the calculations, we took the traffic speed $U_{car} = 10$ m/s, and the traffic intensity $C_{car} = 0.5$ s⁻¹.

Figure 7 shows the flow lines (*a, c*) and isolines of the pollutant concentration (*b, d*) in a street canyon with the following geometric characteristics: $Ly_1 = Ly_2 = 30$ m; $Lx_2 - Lx_1 = 30$ m (see Fig. 1).

The results calculated indicate that the circulating motion of air is formed in the canyon; and the motion

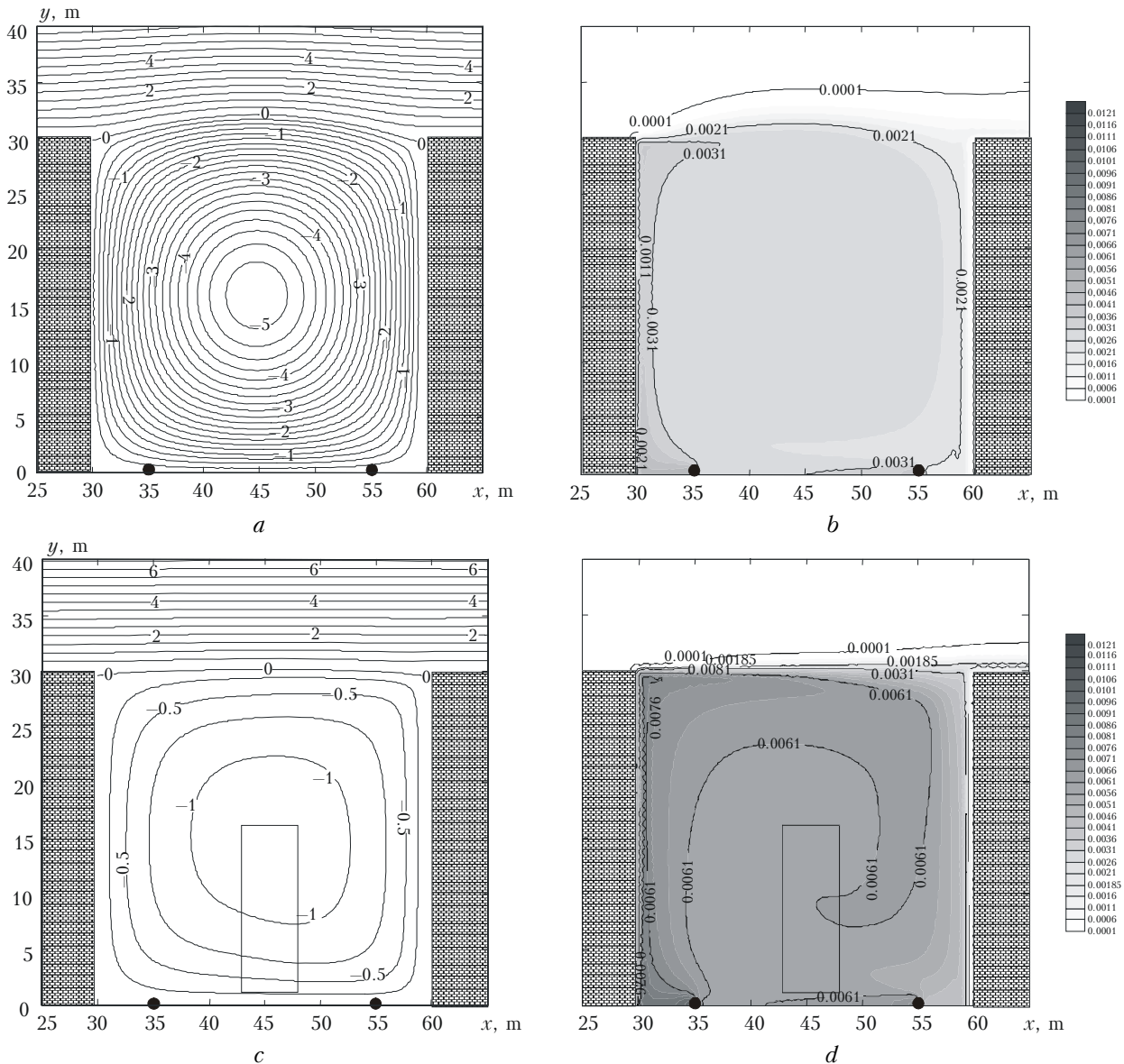


Fig. 7. Flow lines and distribution of the pollutant concentration in the street canyon; $Ly_1 = Ly_2 = 30$ m; $Lx_2 - Lx_1 = 30$ m; the sources of pollutant emission are located at the points $(x = 35, y = 0)$; $(x = 55, y = 0)$; the vegetation area is shown by a rectangle.

direction and intensity are determined by the main flow velocity. The pollutant, emitted by sources located at the canyon bottom and entrained by the circulating motion of air, is transported to the leeward side, and then it is partly carried into the main flow and partly returned into the region bounded by the vertical walls of neighboring buildings. The recirculating flow speed in the canyon is much lower than the air speed above buildings, which favors the formation of the increased level of the pollutant concentration all over the canyon volume and, especially, near the emission sources and near the leeward side of the canyon. It should be noted that the change in the street canyon volume influences the level of air pollution in it,¹⁷ but local maximal values of pollutant concentrations are always observed near the leeward side of the canyon.

A small vegetation area (few pine trees) at the center of the street canyon (Figs. 7c and d; $42.5 \leq x \leq 47.5$ m;

$1 \leq y \leq 15$ m), all other parameters of calculation being the same, significantly decreases the speed of the circulating motion due to the increased resistance to the flow. In addition, the appearance of a penetrable obstacle in the street canyon leads to deformation of flow lines in the vegetation zone and behind it due to lifting motion of air having passed near the obstacle bottom. The intensity of the street canyon ventilation decreases, leading to increase in the level of the pollutant concentration all over the canyon volume and, especially, near the leeward side. The intensification of the turbulent transport caused by a change in the character of the recirculating motion, which shows itself as a lifting turbulized polluted flow behind a penetrable obstacle, favors the additional dispersion of the pollutant.

Figure 8 depicts the flow lines and isolines of the pollutant concentration in a flow around some extended building.

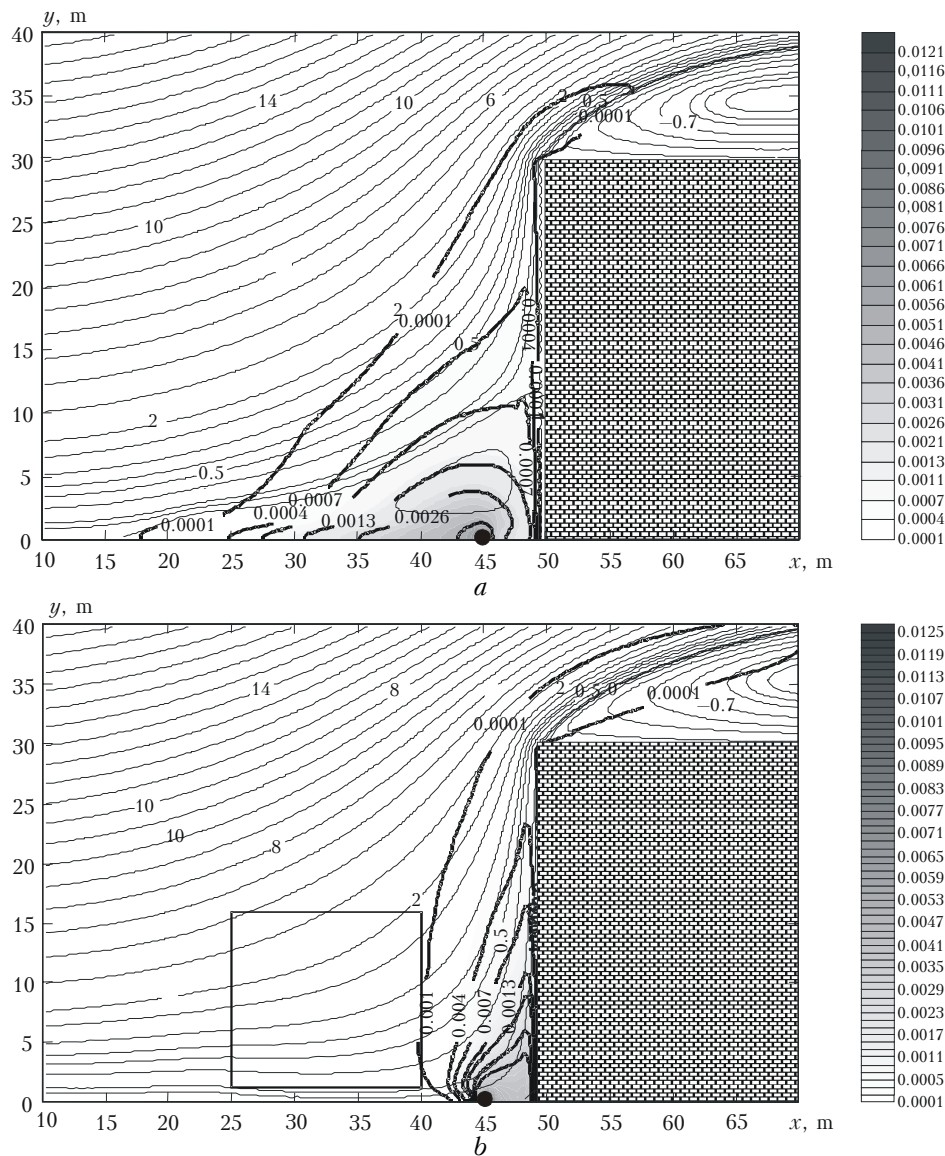


Fig. 8. Flow lines and concentration distribution for a building located on the windward side. $Ly_1 = 0$ m, $Ly_2 = 30$ m; $Lx_1 = 0$ m, $Lx_2 = 50$ m. The source of pollution is located at the point ($x = 45$, $y = 0$); the square shows the vegetation area.

The source of pollution is located 5 m far from the obstacle. The calculated results have shown that two vast recirculating zones are formed in the flow: at the bottom near the windward side of the building and downstream above the building (Fig. 8a). The highest concentrations of the gaseous pollutant are observed in the case, when the roadway is located near the windward side of the building. This can be explained by the fact that, in the region of the recirculating flow, the speed of the air mass motion and the turbulent diffusion are much lower than in the incoming flow and by the presence of the vortex motion, due to which the pollutant continuously circulates in this region and is removed only partly. If the pollution source is located upstream ($x \leq 20$ m), then the pollutant dispersion over the recirculating zone is more intensive due to high turbulent diffusion at this part of the flow.

The presence of a limited vegetation zone (Fig. 8b; $25 \leq x \leq 40$ m; $1 \leq y \leq 15$ m; pine trees) in front of the building changes the aerodynamic pattern of the flow. A penetrable obstacle stabilizes the incoming flow, thus preventing the conditions for formation here of the recirculating flow zone. As a result, the pollutant is mostly transported by the vertical flow and the area of its dispersion becomes much smaller.

Therefore, the level of air pollution near the source under these conditions is higher as compared to the situation shown in Fig. 8a.

Conclusions

We presented a mathematical model and technique of calculation for investigation of aerodynamics in urban building elements. The model was tested and its good agreement with the experimental data has been demonstrated. The distribution of the concentration of a gaseous pollutant emitted by continuous sources, such as traffic, has been calculated in the street canyon and near some isolated building. The influence of a vegetation area located near the urban roadway on the aerodynamic pattern of the flow and the pollutant dispersion has been investigated. Unfavorable

factors, leading to accumulation of harmful pollutants in the surface air and in urban building elements have been revealed.

References

1. T.R. Oke, *Boundary Layer Climates* (Methuen, London, 1987), 435 pp.
2. H. Huang, Y. Akutsu, M. Arai, and M. Tamura, *Atmos. Environ.* **34**, No. 5, 689–698 (2000).
3. P. Louka, M. Ketznel, P. Sahm, E. Guilloteau, N. Moussiopoulos, J.-F. Sini, P.G. Mestayer, and R. Berkowicz, in: *7th Intern. Conf. on Environ. Sci. and Technol.* (2001), No. 9, pp. 1–8.
4. M. Ketznel, R. Berkowicz, and A. Lohmeyer, *Environ. Monitoring and Assess.* **65**, Nos. 1–2, 363–370 (2000).
5. L.G. Loitsyanskii, *Fluid and Gas Mechanics* (Nauka, Moscow, 1987), 840 pp.
6. A. Kimura, T. Iwata, A. Mochida, H. Yoshino, R. Ooka, and S. Yoshida, in: *Summaries of Technical Papers of Annual Meeting Architectural Institute of Japan* (2003), No. 9, pp. 721–722.
7. B.E. Launder and D.B. Spalding, *Computational Methods in Applied Mechanics and Engineering* **3**, No. 2, 269–289 (1974).
8. <http://www2.dmu.dk/AtmosphericEnvironment/trapos/texte/louka-camb.pdf>
9. M.A. Leschziner and W. Rodi, *AIAA Journal* **22**, No. 12, 1742–1747 (1984).
10. S.V. Patankar, *Numerical Heat Transfer and Fluid Flow* (Hemisphere, 1980).
11. B. Noll, *AIAA Journal* **30**, No. 1, 64–69 (1992).
12. A.O. Esaulov and A.V. Starchenko, in: *Computational Fluid Dynamics* (Tomsk State University Press, Tomsk, 1999), pp. 27–32.
13. V.P. Il'in, *Methods of Incomplete Factorization for Solution of Algebraic Systems* (Fizmatlit, Moscow, 1995), 288 pp.
14. *Turbulent Shearing Motions* (Mashinostroenie, Moscow, 1982), Part 1, 432 pp.
15. J. Eichhorn, *MISKAM-Handbuch zur Version 3.x.x. Giese-Eichhorn*. (Wachernheim, Germany, 1998), 55 pp.
16. R. Berkowicz, O. Hertel, S.E. Larsen, N.N. Sørensen, and M. Nielsen, *Modelling Traffic Pollution in Streets* (National Environment Research Institute, Roskilde, Denmark, 1997), 55 pp.
17. R.B. Nuterman and A.V. Starchenko, *Atmos. Oceanic Opt.* **16**, Nos. 5–6, 483–486 (2003).